Advanced Science Letters
Volume 11, Pages 72–79 (30 May 2012)

Electrode Displacement and Dynamic Resistance During Small-Scale Resistance Spot Welding

Yung-Chang Chen[1], Kuang-Hung Tseng[2,*], and Yu-Sheng Cheng[1]

[1]*Department of Vehicle Engineering, National Pingtung University of Science and Technology, Pingtung 91201, Taiwan*
[2]*Institute of Materials Engineering, National Pingtung University of Science and Technology, Pingtung 91201, Taiwan*

Small-scale resistance spot welding (SSRSW) is increasingly being used to join thin sheets and fine wires. It is an important microjoining technique in the fabrication of medical, electronic, and optoelectronic devices. However, maintaining a high quality of nugget is very difficult because SSRSW exhibits highly complex and nonlinear behavior. In this study, a fully coupled thermal-electrical-mechanical finite element model (FEM) was established to provide valuable insight into these complex interactions through computational simulations. FEM simulation not only helps to provide a clearer understanding of the entire welding process, but also enables for the prediction of the formation and growth of a nugget. Moreover, the predicted results are compared with experimental data, and the influences of the electrode displacement and dynamic resistance on the final nugget size are also discussed. This research can provide real-time information useful for monitoring the size of SSRSW nuggets using maximum electrode displacement and minimum dynamic resistance. The results show that the maximum electrode displacement and minimum dynamic resistance serve as important indicators of nugget quality which can directly reflect the formation and growth of nuggets during SSRSW. The data trends clearly show that the final nugget size is directly proportional to the maximum electrode displacement, and inversely proportional to the minimum dynamic resistance.

Keywords: Finite Element Model, Resistance Spot Welding, Electrode Displacement, Dynamic Resistance, Nugget Size.

1. INTRODUCTION

Resistance welding is one of the oldest welding techniques still in use today. It is a fusion welding process which uses the coordinated application of both heat and pressure to produce an adequate weld.[1] The simplest form of this process is resistance spot welding (RSW), in which pressure is provided by clamping two or more metal sheets between two electrodes. Electrical current is then passed between the electrodes for a predetermined time, generating sufficient resistance heat at the sheet/sheet interface or faying surface to cause fusion of the joined sheets, such that a molten nugget is formed between the sheets. In practice, the most common application of RSW is in the automotive industry, where it is used almost universally to join the steel sheets in an automobile.

Recently, SSRSW has been widely used in the fabrication or assembly of medical, electronic, and optoelectronic devices. Note that the difference between "small-scale" and "large-scale" RSW depends not only on sheet thickness, but also on the weld current and electrode force used. SSRSW is used to join thin metal sheets (mostly less than 0.2 mm in thickness) and generate nuggets of a relatively small size, and thus uses a lower weld current and electrode force. However, there remains a lack of understanding of SSRSW despite the increasing demand. By comparison, extensive research has been carried out in the area of large-scale resistance spot welding (LSRSW) of relatively thick metal sheets (mostly greater than 0.6 mm in thickness), mainly for applications in the automotive industry.[2] Compared with LSRSW, limited research has been published for SSRSW in open literature, especially on electrode displacement and dynamic resistance. Moreover, thin sheet resistance welding involves distinct features that pose difficulties in maintaining high quality nuggets.

There are many welding parameters such as weld current, weld time, and electrode force which directly influence the formation and growth of an RSW nugget. Many studies on the nugget size for LSRSW have been conducted[3–6] and it has been found that a shorter threshold time or lower threshold current is required for nugget initiation when the applied electrode force is decreased.[7] Furthermore, the diameter of the nugget formed during welding is generally correlated to the tensile-shear strength of the RSW lapjoint.[8,9] As weld current is increased, the nugget diameter increases with a consequent increase in joint strength. However, exceeding a critical current value leads to a decrease in nugget

*Author to whom correspondence should be addressed.

1936-6612/2012/11/072/008 doi:10.1166/asl.2012.2180

diameter, due to excessive bursts of molten metal (expulsion) from between the sheets.

The size of a nugget is a significant factor in determining RSW quality. The formation and growth of nuggets during RSW depends on the interaction of heat generation and heat dissipation in the lap-joint sheets, which can be characterized by trends in electrode displacement and variables related to dynamic resistance.[10–16] Note that electrode displacement and dynamic resistance can provide the most important information concerning nugget formation and growth during RSW. Electrode displacement is generally regarded as one of the variables that can provide real-time information useful for monitoring RSW quality.[11] Dynamic resistance is the result of the sum of bulk material resistance and contact resistance, and the dominance of each component may change during RSW.[12] In practical terms, controlling process variables requires a solid understanding of how these interactions evolve during welding. Although a tremendous amount of research has been focused on LSRSW process monitoring, the SSRSW process has received less attention because the process variables used for monitoring are very small in magnitude. Note that nugget development during SSRSW is directly influenced by competing process transients. These transients are caused by electrical, thermal, and mechanical interactions, as well as metallurgical phenomena.[8, 17]

The relationship between the RSW variables and nugget size is highly nonlinear and has not yet been systematically studied. Recently, the finite element analysis based computer simulation technique has been proven to be an effective tool for developing an understanding of RSW process in quantitative terms.[18–20] For finite element analysis, LSRSW is generally treated as a large deformation effect; however, the small deformation behavior plays a key role in SSRWS. More detailed studies are required to better understand the effects of electrode displacement and dynamic resistance on the development of nuggets formed during SSRSW. This study investigates the characteristics of nuggets in an SSRSW process for thin stainless steel sheets. A DC transistor type SSRSW machine, equipped with a real-time monitoring system, was employed for this parametric study. To gain insight into SSRSW, a fully coupled thermal-electrical-mechanical finite element model has been developed. The computational results provide the current density distribution and temperature profile, enabling the prediction of nugget development during SSRSW. The predicted results are compared with experimental data, and the influences of electrode displacement and dynamic resistance on the development of a nugget are also discussed.

2. COMPUTATIONAL MODELING

An integrated mathematic model of SSRSW combines the electrode and the sheet. The thermal, electrical and mechanical fields are coupled to analyze the formation and growth of nugget during SSRSW, in which current density distribution is used to calculate heat generation resulting from contact resistance. Current density J_i is expressed as:

$$J_i = -\sigma_{ij}\frac{\partial V}{\partial x_j} \tag{1}$$

where σ_{ij} is the temperature dependent electrical conductivity and V is the electrical potential. Thus, the governing equation for electrical analysis can be described by the Quasi–Laplace equation of current density:

$$\frac{\partial}{\partial x_i}\left(\sigma_{ij}\frac{\partial V}{\partial x_j}\right) = 0 \tag{2}$$

In the electrical-thermal analysis, the amount of heat generated by the Joule effects per unit volume q, can be expressed as:

$$q = \sigma_{ij}\frac{\partial V}{\partial x_i}\frac{\partial V}{\partial x_j} \tag{3}$$

Transient conduction heat transfer of sheets during welding can then be expressed by the following equation:

$$\rho C_p\frac{\partial T}{\partial t} = \frac{\partial}{\partial x_i}\left(K_{ij}\frac{\partial T}{\partial x_j}\right) + q \tag{4}$$

where ρ is the density, C_p is the specific heat per unit volume, K_{ij} is the heat conductivity, and T is the temperature field.

According to elastic mechanics analysis, materials are assumed to be homogeneous and isotropic. Because the mechanical deformation is very small, the displacement equation can be shown to be:

$$(\lambda + G)\frac{\partial e}{\partial x_i} + G\nabla^2 u_i + \left(f_i - \frac{E}{1-2\nu}\frac{\partial \alpha T_d}{\partial x_i}\right) = 0 \tag{5}$$

$$\lambda = \frac{\nu E}{(1+\nu)(1-2\nu)} \tag{6}$$

where G is the shear modulus, e is the total strain, u_i is the amount of deformation, f_i is the body force, E is the Young's modulus, α is the coefficient of thermal expansion, and T_d is the change in temperature.

This study used the commercial software ANSYS to develop a two-dimensional fully coupled multiphysic finite element model to investigate the formation and growth of nuggets during SSRSW. Figure 1 shows a block diagram for the FEM computational procedure. The welding starts with the squeeze stage, in which mechanical force is applied to the electrode and then to the sheets. An initial mechanical status (initial contact area,

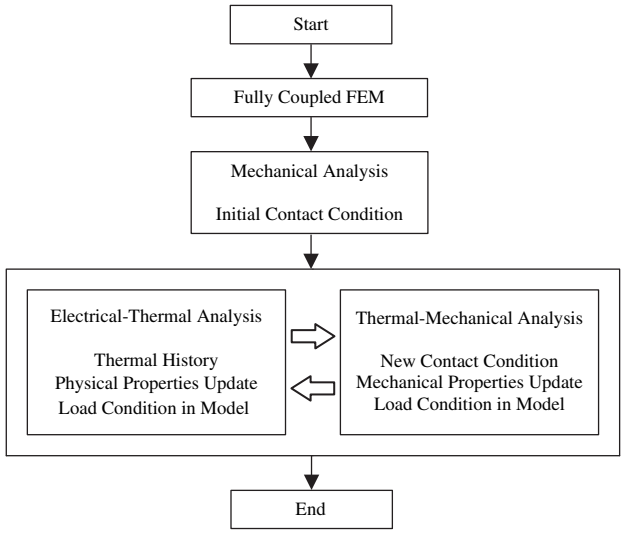

Fig. 1. Schematic diagram of computational procedure.

stress, and deformation distribution) is first analyzed. The interactions between the electrical and thermal fields are then solved simultaneously. An electrical-thermal analysis is used to calculate the Joule heating and temperature development during a small time increment. The calculated temperature field is then imposed into a thermal-mechanical analysis to calculate a new mechanical status, which is updated in the electrical-thermal analysis to account for variations of real contact area. This procedure is repeated and results are updated at each time increment until the welding process is complete.

Only half of the overlap-joint sheet assembly was considered for modeling because of the axial symmetry of the electrode geometry. The model was meshed using three types of elements: a thermoelectric solid element for the electrical-thermal analysis, an isoparametric solid element for the thermal-mechanical analysis, and a surface-to-surface contact element for coupling the two analyses. The mesh structure consists of 550 nodes and 480 elements, which has been shown by a mesh convergence study to provide a sufficiently refined mesh. Figure 2 shows the boundary conditions and loads applied to the model. In the electrical-thermal analysis, the electrical boundary conditions are defined as a zero potential at the bottom end of lower electrode, and a DC potential applied at the top end of upper electrode. At the faying surface and electrode/sheet (*E*/*S*) interface, electrical current is only permitted across areas where the faying surface and *E*/*S* interface are in contact, while no current flow is allowed when these surfaces are separated. In the thermal–mechanical analysis, electrode force is applied as an evenly distributed pressure at the top end of upper electrode. The axial displacements at the bottom end of lower electrode, together with the radial displacements of the central line, are all constrained.

For computational simulation of welding processes, material modeling is a key factor, according to the ANSYS theory manual. In coupled thermal-electrical-mechanical analysis, a nonlinear model that includes a transient computational approach was adopted, in which the material properties were considered as a function of temperature. Also, the thermal contact conductivity (TCC) and electrical contact conductivity (ECC) were imposed as temperature-dependent at the faying surface and *E*/*S* interface. Figure 3 shows the thermophysical and mechanical properties as functions of temperature for the sheet materials used. The melting point of the sheet materials was chosen to be 1400 °C. Furthermore, no phase transformation occurred in austenitic stainless steel molten metal during SSRSW. Tekriwal and Mazumder reported that the influence of temperature on the Poisson ratio may be neglected.[21] Therefore, the Poisson ratio was assumed to maintain a constant value of 0.28.

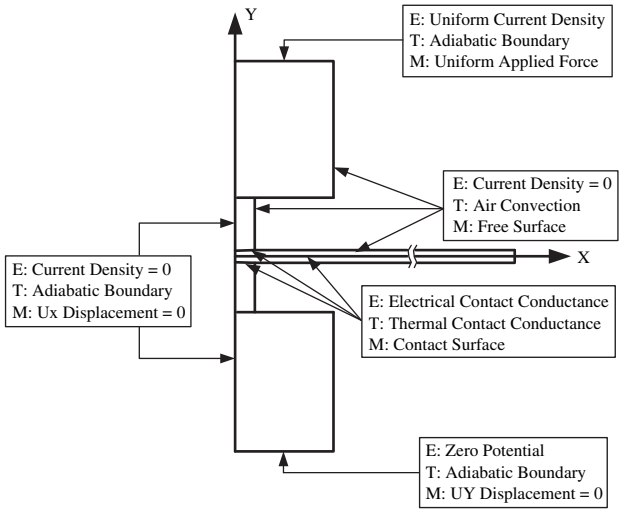

Fig. 2. Computational domain and boundary conditions for finite element model.

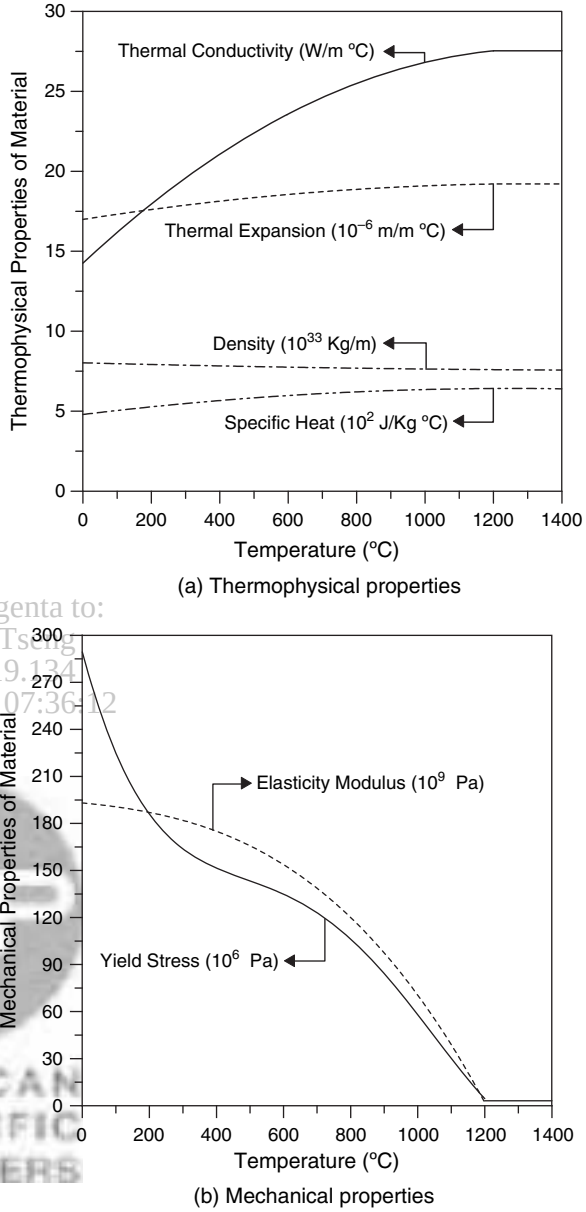

Fig. 3. Variation of material properties with temperature of test specimen.

3. EXPERIMENTAL DETAILS

Commercial stainless steel AISI 301 sheets were selected as test specimens. The chromium-nickel austenitic alloy steels have very high electrical resistances and are readily joined by SSRSW. Table I shows the chemical composition of the material used. Sheets of thickness 0.1 mm were cut into 30 × 10 mm strips,

Table I. Chemical composition (wt%) of AISI 301 stainless steel.

C	Si	Mn	P	S	Cr	Ni	Fe
0.15	0.52	1.29	0.045	0.03	17.3	6.7	Bal.

roughly polished using 400 grit silicon carbide papers to remove surface contamination, and then cleaned with acetone. All tests were performed using a standard RWMA Class II Cu-Cr alloy electrode with a flat surface and a 1.2 mm tip diameter. Figure 4 illustrates the geometry and dimensions of the electrodes and an overlap-joint sheet. No water was used to cool the electrodes because of the limited electrode dimensions in SSRSW.

A DC transistor type SSRSW machine was equipped with a PC-based monitoring system capable of simultaneously recording force, displacement, current, and voltage as functions of time. This system enables the automatic retrieval of force and displacement values for the upper electrode at every time step during welding. The electrode force was controlled using an electromagnetic motor. During SSRSW, measuring electrode displacement is difficult because the magnitude is very small. In this work, a laser displacement sensor was used to detect displacement of the upper electrode. The experimental setup used in this study is shown in Figure 5. The PC, linear solenoid, and force sensor form a feedback system to control the movement of the upper electrode during SSRSW welding. Maximum rated output current of the SSRSW machine is 400 A. This machine has a constant current power amplifier which can be controlled using the PC. The PC central controller has four input signals and two control outputs. The input signals include current, voltage, electrode force, and displacement, and the control outputs include a solenoid current controlling signal to drive the electrode and a weld current controlling signal to drive the machine. During SSRSW welding, the voltage across and current through the electrode tip were recorded to calculate the dynamic resistance. For the sake of accuracy, a PC with MATLAB was employed to manage all of the process variables.

Welding parameters used in the present study are given in Table II. Three measurements were taken and the results averaged for each test condition. Cross-sections of SSRSW nuggets were characterized using an optical microscope, and measurements of nugget size were made from the resulting macrographs. Furthermore, the measured nugget size obtained from the experimental work was compared systematically with the predicted results.

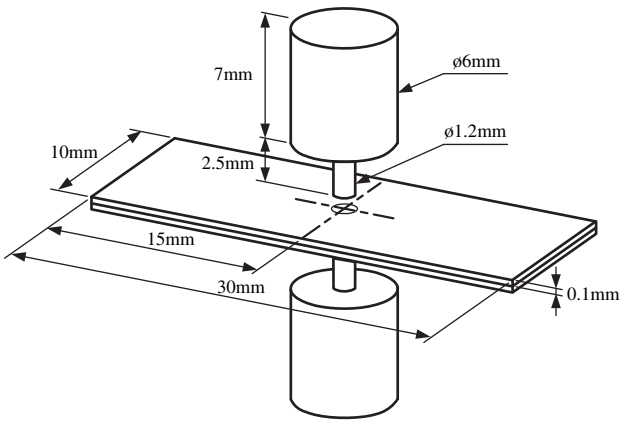

Fig. 4. Geometry and dimensions of electrode and sheet used in this study.

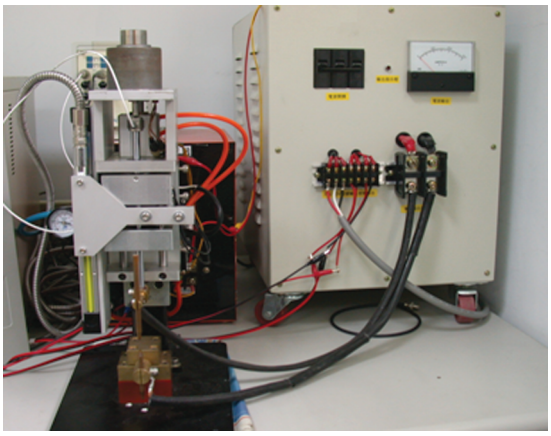

Fig. 5. Experimental setup for SSRSW.

4. RESULTS AND DISCUSSION

4.1. Contact Pressure Distribution

Determining the contact pressure at the faying surface is a critical issue for the computational simulation of SSRSW, since the contact pressure distribution at the faying surface influences the mechanisms of nugget formation and growth. Figure 6 shows the contact pressure distribution of the faying surface at different squeeze times. When the upper electrode contacts the lap-joint sheet, an impact pressure occurs. The distribution of contact pressure is not uniform along the faying surface, and the largest pressure occurs near the center of the faying surface. A larger contact pressure results in a lower contact resistance, tending to increase current density. As a result, the distributions of contact resistance and current density at the faying surface are strongly related to changes in the contact pressure.

As is well known the squeeze time is when the two electrodes come together and the lap-joint sheet is compressed between the electrodes the compression force is built up to a specified amount before the weld current is applied to the sheets. Too short a squeeze time may result in an unconformable nugget. In order to ensure a desired size of the nugget, a sufficient pre-welding squeeze time is necessary to delay the weld current until the applied electrode force has reached the desired level. Furthermore, the squeeze time needed to reach a stable contact pressure distribution remains fairly constant. As can be seen from Figure 6, increasing the duration of squeeze can assure that the electrode pressure is stable in the SSRSW process.

4.2. Nugget Formation and Growth

In RSW, the size of the nugget formed during welding is generally correlated to the strength of the lap-joint, and is therefore used as a key quality criterion in production.[22] Figure 7 shows typical nugget formation and the growth curve obtained from the computational analysis. The nugget develops very rapidly and

Table II. Welding parameters for SSRSW experiment.

Electrode pressure (MPa)	Weld current (A)	Squeeze time (ms)	Weld time (ms)	Hold time (ms)
1, 3.3, 5	250, 270, 300, 320, 350	5, 10, 15, 20, 40	100	30

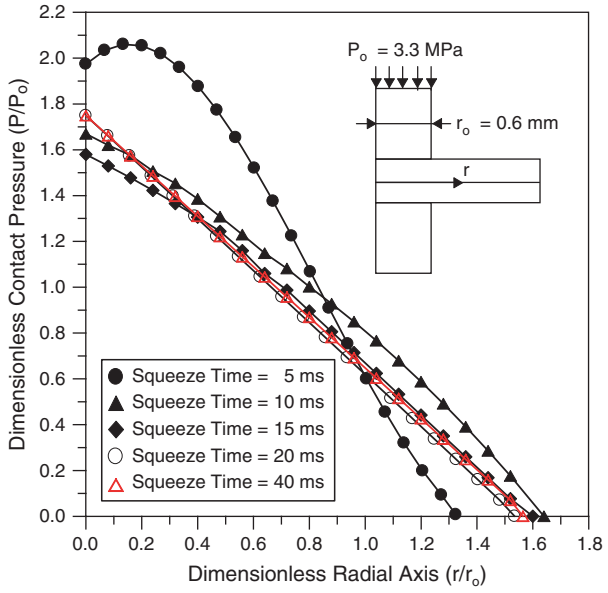

Fig. 6. Contact pressure distribution of faying surface at different squeeze times.

reaches its maximum size within a very short weld time. Further increases in the hold time will not significantly increase the nugget size. During RSW, the heat generation is directly proportional to the weld current and weld time. Due to the heat transfer from the molten zone to the sheets and to the electrodes, as well as the heat loss from the free surfaces to the surroundings, a minimum weld current and weld time are necessary to form a nugget. In other words, the nugget formation and growth as a function of weld current and weld time occurs in three stages:

(i) no melting occurs and a nugget is not formed during the squeezing period;

(ii) nugget formation and rapid nugget growth stage during the welding period;

(iii) slow nugget growth rate stage during the holding period.

As is well known, the peak temperature was at the center of the faying surface, and the temperature of the faying surface exceeded that of the *E*/*S* interface. Consequently, the growth rate of the nugget diameter is much greater than that of nugget thickness. A deeper understanding of the mechanisms that govern nugget formation and growth could provide the development of more efficient FEM analyses for the SSRSW process.

4.3. Effect of Welding Parameters on Electrode Displacement

Electrode displacement is most commonly used for monitoring nugget quality in RSW.[11, 13–15] However, the influence of parameters for SSRSW on electrode displacement has not been well documented. Figure 8 shows a displacement-time curve of the upper electrode during SSRSW. It is well accepted that electrode displacement is due to the interaction between the thermal expansion of the sheet and the mechanical constraints of the electrode. As the weld current is applied after squeezing, the electrode displacement rapidly increases due to the thermal expansion of sheet, and then gradually decreases during the cooling stage when the weld current is terminated. A comparison of Figures 7 and 8 indicates that, under the same electrode force, weld current, and weld time, a peak of the electrode displacement curve is observed and is believed to be relevant to the formation of a sufficiently sized nugget. As a result, the trace of the displacement-time curve of an electrode is an ideal monitoring parameter capable of directly indicating the formation and growth of nuggets during SSRSW.

The influence of weld current and electrode force on the maximum electrode displacement is shown in Figure 9. The maximum electrode displacement is directly proportional to the weld current and is inversely proportional to the electrode force. Results obtained from computational analysis are consistent with monitored readings. The change in weld current is a response to the thermal expansion of the sheets. It is well known that the higher the weld current, the greater the heat energy produced. As weld current increases, the expansion rate of the sheet increases. The

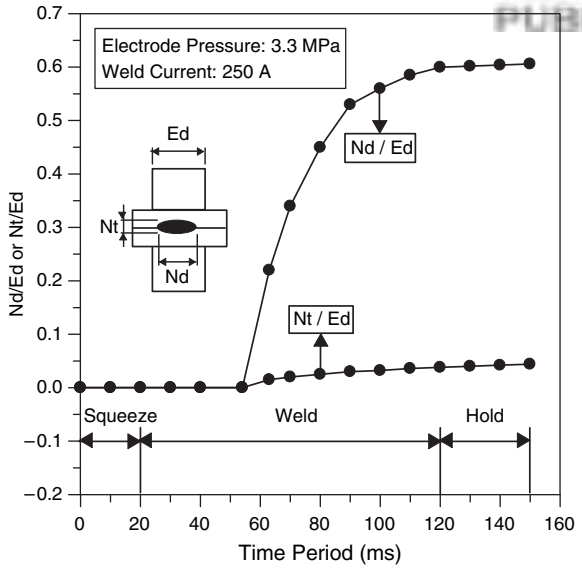

Fig. 7. Nugget formation and growth curve during SSRSW.

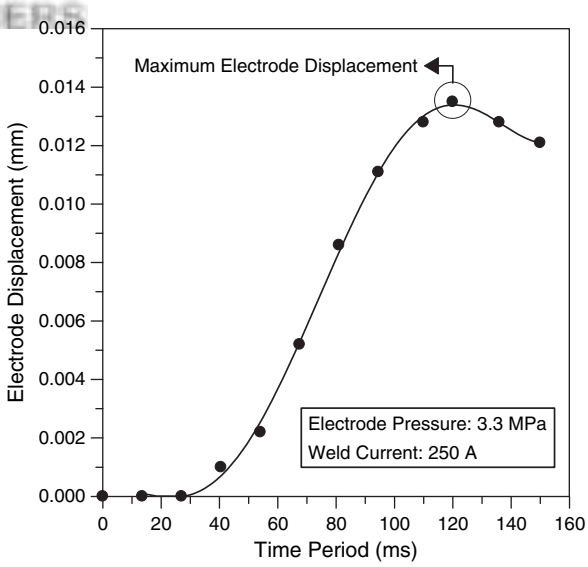

Fig. 8. Electrode displacement-time curve during SSRSW.

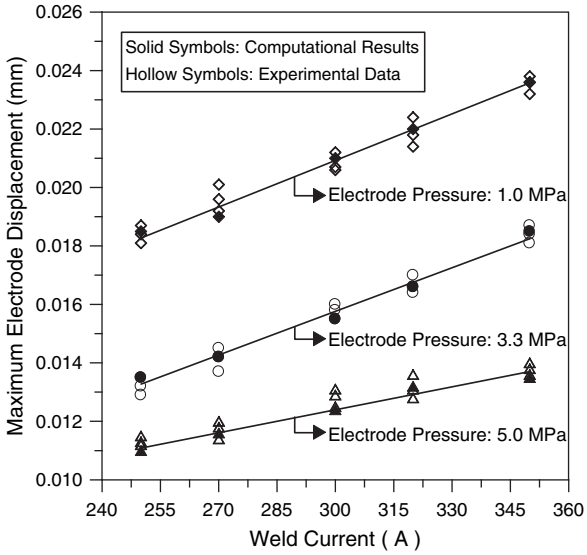

Fig. 9. Effect of weld current and electrode force on maximum electrode displacement.

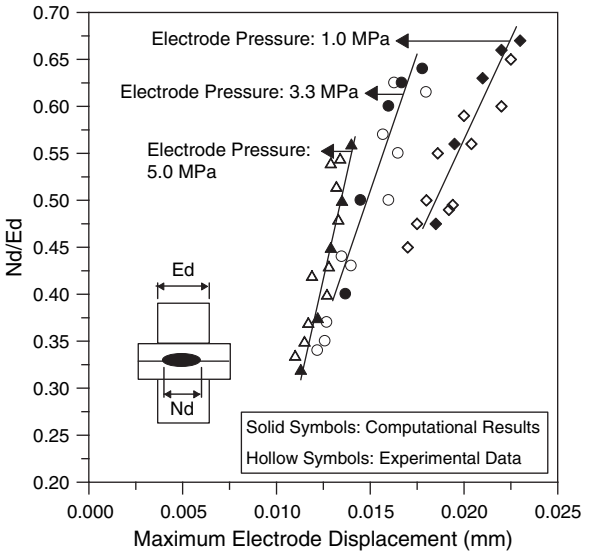

Fig. 10. Variation in diameter of nugget with maximum electrode displacement.

maximum electrode displacement therefore also increases under the same electrode force conditions. Note that if the applied heat input becomes too high, the molten nugget will overdevelop, resulting in expulsion.

The change in electrode force is a response to the sheet's deformation under mechanical constraints. It is well known that a higher electrode force results in a higher clamping ability. As electrode force increases, the amount of deformation of the sheet decreases. The maximum electrode displacement therefore decreases as well. On the other hand, a higher electrode force will result in an increased contact area and hence a reduced current density at the faying surface, which in turn decreases the maximum displacement of the upper electrode during SSRSW under the same weld current conditions. Note that if the applied electrode force is too low, expulsion may occur immediately after starting the weld current due to the excessively high contact resistance at the faying surface, resulting in rapid heat generation.

4.4. Relationship of Maximum Electrode Displacement and Nugget Size

Figures 10 and 11 show the variations in nugget size with maximum electrode displacement. With an increase in maximum electrode displacement, the diameter and thickness of SSRSW nuggets also increased linearly under the same electrode force conditions. In other words, the trends of these data clearly showed that the final nugget size is directly proportional to the maximum electrode displacement. Based on the experimental results, the relationship has a correlation coefficient of 0.8866 for nugget diameter, and 0.9349 for nugget thickness. It is evident that electrode displacement is a result of thermal expansion when the sheet is heated by the weld current. Therefore, the final nugget size is strongly correlated with the peak value of an electrode displacement curve. Moreover, it is expected that the nugget thickness is more sensitive than the nugget diameter to electrode displacement. In other words, the maximum electrode displacement is more closely correlated to nugget thickness than to nugget diameter.

4.5. Relationship of Minimum Dynamic Resistance and Nugget Size

Dynamic resistance is one of the most critical physical properties in RSW, determining the heat generation during welding and the subsequent nugget development.[23] Although there have been a number of investigations into dynamic resistance for mild steels, those for stainless steels are limited. The dynamic resistance curve in RSW for mild steel has a typical shape: the resistance drops sharply at the beginning, and then rises; before the weld current is terminated, the resistance starts to drop, which results in a peak.[15] The resistance traces at different time conditions in SSRSW for stainless steel are shown in Figure 12. This represents the total resistance of the secondary electrical circuit. It is well known that when the lap-joint sheet is pressed by the electrodes, local contact is initially established through faying

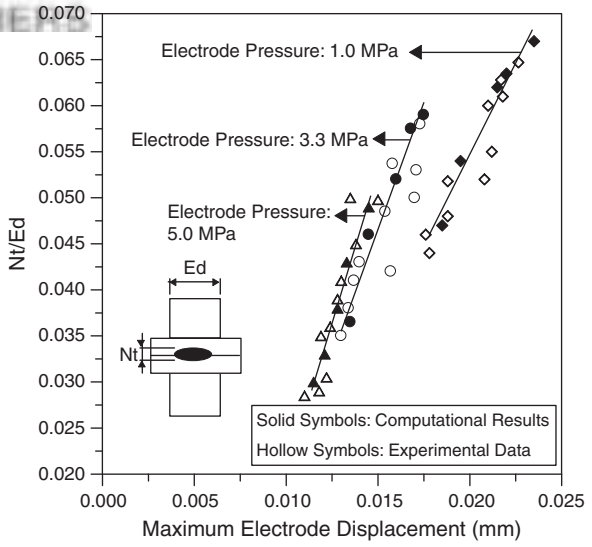

Fig. 11. Variation in thickness of nugget with maximum electrode displacement.

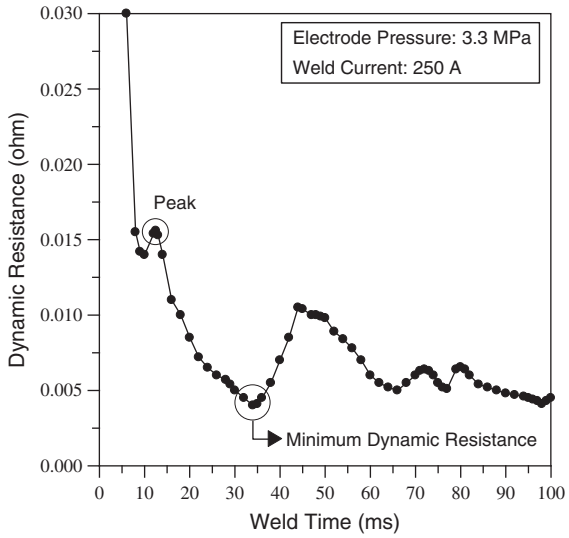

Fig. 12. Dynamic resistance-time curve during SSRSW.

surface asperities. Dynamic resistance begins decreasing rapidly due to the collapse of faying surface asperities. The effect of rising temperature then results in an increase in bulk material resistance. While it reaches a peak, the effect of an increase in contact area results in the contact resistance falling to a minimum value. In other words, the peak in the dynamic resistance-time curve is a result of the competing effects of bulk material resistance increase with increasing temperature and contact resistance decrease with asperity breakdown and sheet softening. Following the formation of a nugget at the faying surface, the dynamic resistance again increases.

Traditionally, several factors based on dynamic resistance patterns have been extracted and used to estimate the quality of RSW nuggets. In this work, an exact minimum dynamic resistance, which is related to the initial formation of the molten nugget, is selected as the only geometric extraction factor to simplify the correlating process. It is believed that the minimum dynamic resistance dominates changes in the contact area, and thus the final nugget size. Variation in nugget size with the minimum dynamic resistance is shown in Figure 13. With an increase in minimum dynamic resistance, the diameter and thickness of SSRSW nuggets decrease. In other words, the trends of these data clearly show that the final nugget size is inversely proportional to the minimum dynamic resistance. The minimum dynamic resistance is almost proportional to the diameter and thickness of nugget, with correlation coefficients of −0.8618 and −0.8289, respectively. As a result, in SSRSW of stainless steels, the minimum dynamic resistance can be considered an effective process variable with which to correlate the nugget size.

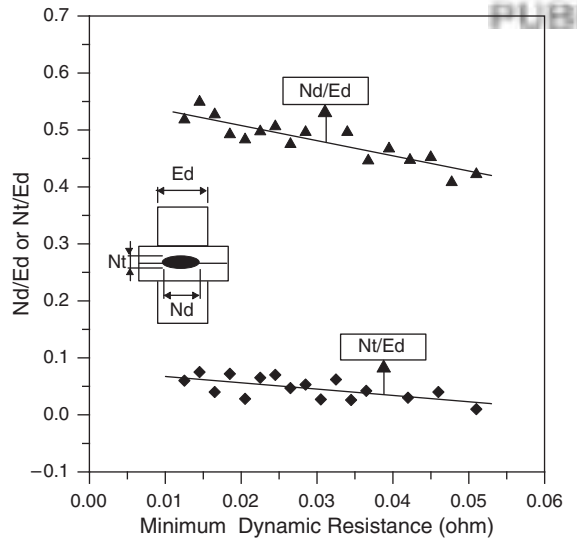

Fig. 13. Variation in diameter and thickness of nugget with minimum dynamic resistance.

5. CONCLUSIONS

Consistently producing a high quality of nugget using SSRSW is not easy, and the quality is generally characterized by nugget size. SSRSW of thin stainless steel sheets was studied in order to characterize the influence of maximum electrode displacement and minimum dynamic resistance on the final nugget size. Computational results were compared with experimental data and the major research conclusions are listed below:

(1) The distribution of contact pressure is not uniform along the faying surface, and the largest pressure occurs near the center of the faying surface. Furthermore, the squeeze time needed to reach a stable contact pressure distribution remains fairly constant.

(2) Nugget development occurs very rapidly and reaches its maximum size within a very short weld time. Further increasing the hold time will not obviously increase the nugget size. In SSRSW, the temperature of the faying surface exceeded that of the *E*/*S* interface. Consequently, the growth rate of nugget diameter exceeded that of nugget thickness.

(3) A peak of the electrode displacement-time curve is believed to be relevant to the formation of a sufficiently sized nugget. Furthermore, the maximum electrode displacement is directly proportional to the weld current and is inversely proportional to the electrode force. The change in weld current is a response to the thermal expansion of the sheet. However, the change in electrode force is a response to the sheet deformation under mechanical constraints.

(4) The maximum electrode displacement and minimum dynamic resistance serve as important indicators of nugget quality which can directly reflect the formation and growth of nuggets during SSRSW. The data trends clearly show that the final nugget size is directly proportional to the maximum electrode displacement, and inversely proportional to the minimum dynamic resistance.

Acknowledgments: The authors gratefully acknowledge the financial support for this research provided by the National Science Council, Taiwan, Republic of China, under the Grant No. 99-2221-E-020-006.

References and Notes

1. K. H. Tseng and Y. C. Chen, *Key Eng. Mater.* 480–481, 427 **(2011)**.
2. N. Harlin, T. B. Jones, and J. D. Parker, *J. Mater. Process. Technol.* 143–144, 448 **(2003)**.
3. M. Pouranvari, H. R. Asgari, S. M. Mosavizadch, P. H. Marashi, and M. Goodarzi, *Sci. Technol. Weld. Join.* 12, 217 **(2007)**.

4. M. Shome and S. Chatterjee, *ISIJ Int.* 49, 1384 **(2009)**.
5. N. Ma and H. Murakawa, *Trans JWRI* 38, 19 **(2009)**.
6. H. Eisazadeh, M. Hamedi, and A. Halvaee, *Mater. Des.* 31, 149 **(2010)**.
7. B. H. Chang and Y. Zhou, *J. Mater. Process. Technol.* 139, 635 **(2003)**.
8. Y. Zhou, P. Gorman, W. Tan, and K. J. Ely, *J. Electron. Mater.* 29, 1090 **(2000)**.
9. L. Han, M. Thornton, D. Boomer, and M. Shergold, *J. Mater. Process. Technol.* 211, 513 **(2011)**.
10. A. De and M. P. Theddeus, *Sci. Technol. Weld. Join.* 7, 111 **(2002)**.
11. J. Z. Chen and D. F. Farson, *Meas. Sci. Technol.* 15, 2419 **(2004)**.
12. W. Tan, Y. Zhou, H. W. Kerr, and S. Lawson, *J. Phys. D: Appl. Phys.* 37, 1998 **(2004)**.
13. J. Z. Chen, D. F. Farson, K. Ely, and T. Frech, *Int. J. Adv. Manuf. Technol.* 27, 672 **(2006)**.
14. H. Wang, Y. S. Zhang, and G. L. Chen, *Measurement* 42, 1032 **(2009)**.
15. J. Wen, C. S. Wang, G. C. Xu, and X. Q. Zhang, *ISIJ Int.* 49, 553 **(2009)**.
16. X. F. Wang, Y. B. Li, R. H. Li, and G. X. Meng, *Sci. Technol. Weld. Join.* 16, 140 **(2011)**.
17. P. Chigurupati, B. K. Chun, A. Bandar, and W. T. Wu, *Int. J. Mater. Form.* 3, 991 **(2010)**.
18. X. Sun and M. A. Khaleel, *Weld. J.* 83, 197s **(2004)**.
19. H. Zhigang, I. S. Kim, J. S. Son, H. H. Kim, J. H. Seo, K. C. Jang, D. K. Lee, and J. M. Kuk, *J. Achieve Mater. Manuf. Eng.* 14, 140 **(2005)**.
20. J. C. Tan, S. A. Westgate, and T. W. Clyne, *Sci. Technol. Weld. Join.* 12, 490 **(2007)**.
21. P. Tekriwal and J. Mazumder, *J. Eng. Mater. Technol.* 113, 336 **(1991)**.
22. C. T. Ji and Y. Zhou, *J. Manuf. Sci. Eng.* 126, 605 **(2004)**.
23. M. Rashid, J. B. Medley, and Y. Zhou, *Can. Metall. Quart.* 50, 61 **(2011)**.

Received: 25 August 2011. Accepted: 9 October 2011.